frontiers in Earth Science

ORIGINAL RESEARCH
published: 09 December 2020
doi: 10.3389/feart.2020.542116

Insights Into the Internal Dynamics of Natural Lahars From Analysis of 3-Component Broadband Seismic Signals at Volcán de Colima, Mexico

Braden Walsh[1,2]*, *Velio Coviello*[3], *Lucia Capra*[4], *Jonathan Procter*[5] and *Victor Márquez-Ramirez*[4]

[1]Department of Earth Sciences, Uppsala University, Uppsala, Sweden, [2]Centre of Natural Hazards and Disaster Science, Uppsala University, Uppsala, Sweden, [3]Faculty of Science and Technology, Free University of Bozen-Bolzano, Bolzano, Italy, [4]Centro de Geociencias, Universidad Nacional Autónoma de México, Querétaro, Mexico, [5]Volcanic Risk Solutions, Institute of Agriculture and Environment, Massey University, Palmerston North, New Zealand

OPEN ACCESS

Edited by:
Elaine Spiller,
Marquette University, United States

Reviewed by:
Vern Manville,
University of Leeds, United Kingdom
Patricia Ann Mothes,
Escuela Politécnica Nacional, Ecuador
Mark Thomas,
University of Leeds, United Kingdom
Patrick J Smith,
Dublin Institute for Advanced Studies (DIAS), Ireland

***Correspondence:**
Braden Walsh
braden.walsh@geo.uu.se

Specialty section:
This article was submitted to Volcanology, a section of the journal Frontiers in Earth Science

Received: 11 March 2020
Accepted: 18 November 2020
Published: 09 December 2020

Citation:
Walsh B, Coviello V, Capra L, Procter J and Márquez-Ramirez V (2020) Insights Into the Internal Dynamics of Natural Lahars From Analysis of 3-Component Broadband Seismic Signals at Volcán de Colima, Mexico. Front. Earth Sci. 8:542116. doi: 10.3389/feart.2020.542116

Lahar monitoring on active volcanoes is challenging, and the ever changing environment leads to inconsistent results that hamper a warning systems ability to characterize the flow event properly. Therefore, more data, new methods, and the use of different sensors needs to be tested, which could lead to improvements in warning capabilities. Here, we present data from a 3-component broadband seismometer and video camera installed 3 m from the Lumbre channel on Volcán de Colima, Mexico to understand rheology differences within multiple lahar events that occurred in late 2016. We examine differences in frequency and directionality from each seismic component. Results indicate an increase in peak frequency above background in each component when a lahar nears the sensor, and a decrease in overall peak frequency when transitioning from a streamflow to a higher concentration flow. The seismic frequency distribution for the cross-channel component for the streamflow has a wider range compared with the lahar events. In contrast, the peak spectral frequency of the streamflow is narrower in comparison to the lahar events in the flow parallel and vertical directions. Estimated directionality ratios (cross-channel signal divided by flow parallel signal) yielded further evidence for a rheologic change between streamflow and lahars. Directionality ratios >1 were calculated for each lahar, and <1 for streamflow. Finally, we demonstrate from component analyses that channelization or freedom of movement in the cross-channel, bedload transport in the flow parallel, and bed composition in the vertical directions are possibly the main drivers in the peak spectral frequency output of lahars. The results described here indicate that using all three components may provide important information about lahar dynamics, which may be useful for automatic detection and warning systems, and using all three components should be encouraged.

Keywords: lahar dynamics, directionality, volcán de colima, peak spectral frequency, volcanic mass flow, 3-component seismic monitoring

INTRODUCTION

Seismic monitoring techniques are convenient for characterizing fluvial processes because they can provide continuous data at safe distances from the channel (Coviello et al., 2019; Hürlimann et al., 2019). However, correct interpretation of the seismicity induced by flow processes depends on many factors related to source and medium characteristics. Particularly, when describing what factors contribute to the frequency content generated by a flow, there are four main categories: dynamics of the suspended fraction, mechanics of the coarse fraction, properties of the solid-fluid mixture, and channel bed properties. The dynamics of the suspended fraction (e.g. size, concentration, distribution) have been shown to affect the frequency of the seismic signals in multiple ways (e.g. Tsai et al., 2012; Turowski et al., 2015). Doyle et al. (2010) noted when the concentration increases, the frequency will decrease. Furthermore, if there are larger clasts suspended in the flow, increasing the grain size distribution will produce a wide frequency range (Huang et al., 2004). Mechanics of coarse fraction factors (e.g. frictional effects, collisions, bedload) have varying effects on the frequency spectra (e.g. Doyle et al., 2011; Gimbert et al., 2014). It has been shown that the bedload is positively correlated with the amplitude of the frequency spectra, in that an increase in bedload transport will increase the amplitude of the frequency spectra (Coviello et al., 2018) and create higher peak frequencies (Schmandt et al., 2017). Furthermore, Huang et al. (2004) showed that frictional processes produce lower frequency ranges than particle collisions. Properties of the solid-fluid mixture (e.g. turbulence, velocity, viscosity, density) play a significant role in determining the frequency signature of flows (e.g. Cole et al., 2009; Barriere et al., 2015; Coviello et al., 2019). Huang et al. (2004) noted that the high frequency content dampens when the flow contains slurry, indicating that when the viscosity increases, the dominant frequency will be lower. Additionally, Doyle et al. (2010) showed that laminar high concentration flows have lower frequencies than turbulent ones. Similarly, Gimbert et al. (2014) found that turbulence has lower frequencies than bedload processes. Finally, channel bed properties (e.g. geometry, composition, wetted perimeter) can also have an impact on the spectral frequency of a flow (e.g. Doyle et al., 2010; Coviello et al., 2018). Kean et al. (2015) noted the composition of the channel bed can have significant impact on ground vibrations, which can lead to differences in the frequency spectra. For example, a bed made up of gravel or fine sediments will decrease the frequency of the seismic signal compared to a smooth surface (Huang et al., 2004). The density of the channel bed is important as well. Huang et al. (2007) showed that the frequency range will narrow when the bed surface is denser. Furthermore, the greater the wetted perimeter, the more effect the flow will have on the cross-channel signals (Doyle et al., 2010).

As mentioned above, seismic sensors have been used to estimate flow processes of mass flows many times previously. These studies have shown that inconsistent and non-universal results impede hazard assessment of mass flows. This indicates the need for new data processing techniques and more data to make interpretations more reliable. One such technique is to use all three components of the seismometer to study the seismic response of mass flows. Recently, others have used all three components while recording mass flows, including snow avalanches (Kogelnig et al., 2011), streamflow (Roth et al., 2016), hyperconcentrated flows (Walsh et al., 2016), landslides (Surinach et al., 2005), and snow-slurry lahars (Cole et al., 2009). By using all three components, full assessment of the overall properties of the flows can be completed to yield useful information about mass flow processes, particularly in the frequency domain, which may lead to better real-time monitoring and hazard evaluation.

Lahar monitoring on active volcanoes is a challenging task, and past work recording and characterizing the dynamics of natural lahars with 3-component seismometers base their conclusions off of only a few observed events at the same location in a limited time span. For example, Doyle et al. (2010) recorded eight events, only one of which was described seismically. Cole et al. (2009) recorded only two events, each with contrasting characteristics. Additionally, Doyle et al. (2011) describes only three events, which are the same as the events from Doyle et al. (2010). The reason for only a small amount of recordings is due to the limited amount of permanent monitoring stations that continually record lahars worldwide (e.g. Thouret et al., 2020). Conversely, natural lahar events are rarely recorded on channel side instrumentation in such robust detail as on Volcán de Colima. Nevertheless, even at Volcán de Colima, the continual installment of a 3-component seismometer is not possible, and the short duration of the monitoring in 2016 as shown here reinforces the idea that there is a need for a greater amount of lahar events recorded by 3-component broadband seismometers to adequately define either a detailed rheology classification of events or a robust quantification of internal dynamics. However, the identification of some unique features of flow events can still be theorized and shown with the limited amount of data presented here and in past publications.

Volcán de Colima (**Figure 1**) is one of the most active volcanoes in Mexico, which produces a wide range of primary eruptive and secondary non-eruptive hazards (Capra et al., 2018). The channels of the volcano often produce multiple flow events of different rheologies every rainy season that can travel great distances and cause damage to the surrounding infrastructure (Capra et al., 2010). These flow events are considered lahars and are defined as rapidly-flowing mixtures of poorly sorted rock, water, sediment, and mud flowing downslope from a volcano (Pierson, 1985; Calvari et al., 1998). Almost all of the lahars flow down one of the five main channels of Volcán de Colima (Cordobán, Arena, Lumbre, Montegrande, San Antonio), with Lumbre and Montegrande channels containing the most flow events (Coviello et al., 2018). Lumbre is the largest channel system on the volcano encompassing ~14 km^2 (Capra et al., 2018). Therefore, in 2014 a lahar monitoring station was installed (**Figure 1**) on the left bank of the channel (~7 m high) at ~1,580 m above sea level. The monitoring station is comprised of a vertical geophone and camera, where the channel is ~30 m across and slopes at ~6° (Coviello et al., 2018). Later, in

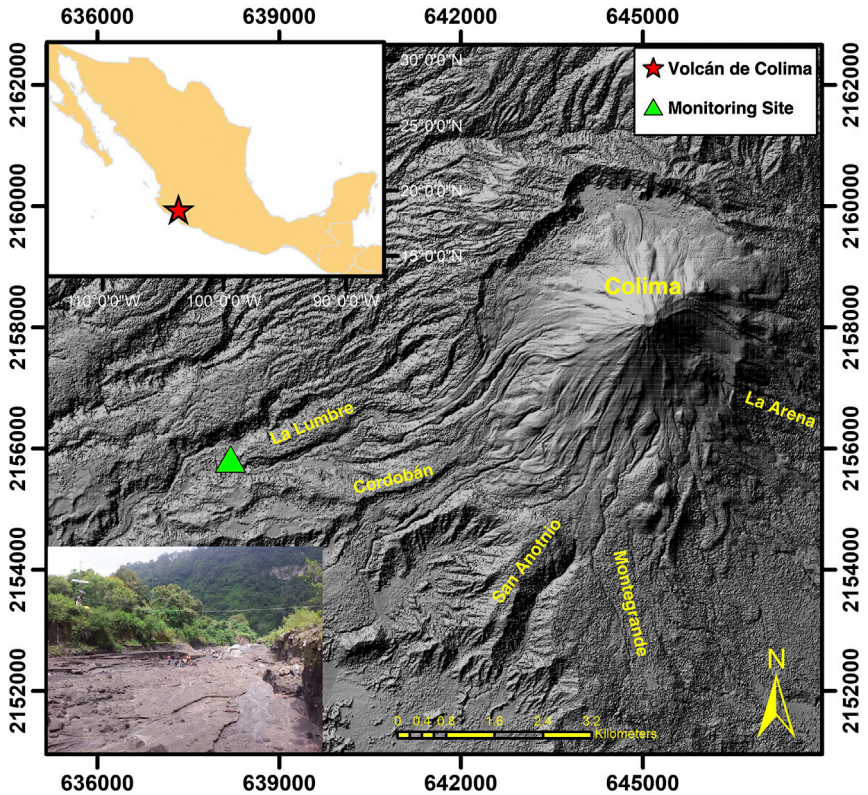

FIGURE 1 | Map of Vocán de Colima showing the five main lahar channels. Green triangle is the location of the monitoring site along the Lumbre channel used in this study, where a broadband 3-component seismometer and camera are installed. Inset picture shows the location of the monitoring station (pictured left) along the channel looking downstream.

2016, a 3-component broadband seismometer was installed for approximately three months at the same location.

2016 Lahar Events

In 2016 there were four lahar events that were recorded by the 3-component seismometer on Lumbre (August 26, 29, 30, September 9), with the larger two (August 26 and 30) contrasting in nature. The lahar on August 26 occurred during sunny conditions at the monitoring site with no precursory flow or sustained flowing water in the channel (these precursory conditions will henceforth be referred to as dry channel). The lahar passed the monitoring station at approximately 22:07:47 UTC (determined by video) and continued for ~40 min. The lahar started as a surge with a large frontal head (30 m wide with a velocity of ~12 m/s), which over time incised the channel bed creating a secondary channel, and was able to move and emplace large boulders up to 5 m in size.

The August 30 event differed from the other three lahars by the presence of a dilute precursory flow before the main lahar phase that lasted ~1.7 h altogether. The precursory streamflow started to pass the Lumbre station at approximately 22:52:53 UTC at a velocity of ~2.8 m/s with the lahar head arriving at 23:09:58 with a frontal velocity of ~9.6 m/s. Additionally, the August 30 event deposited fine-grained volcanic material in the channel, enough to cover the large boulders emplaced by the August 26 event.

The August 29 and September 9 events were smaller in size compared to the August 26 and 30 events. The August 29 lahar was a dry channel slow moving (frontal velocity of ~1.9 m/s) hyperconcentrated flow, which passed the monitoring station at 23:45:30 UTC, lasted ~1.5 h, and was contained within the August 26 incised channel. The September 9 event occurred overnight, reached the seismometer at 01:02:00 UTC and lasted ~1.4 h. The lahar event occurred in a dry channel with a frontal velocity of ~4.7 m/s and flowed over the fresh fine-grained material deposited by the August 30 event.

DATA

The seismic data for the 2016 lahars were recorded on a Nanometrics Trillium 120 s 3-component broadband seismometer, which was installed 3 m from the left bank (downstream) of the Lumbre channel. The station recorded data at 100 Hz sampling and had GPS time-stamps. The broadband seismometer axes were aligned with the lahar channel specifying the North-component pointed upstream as flow parallel (P) and the East-component as the cross-channel (T)

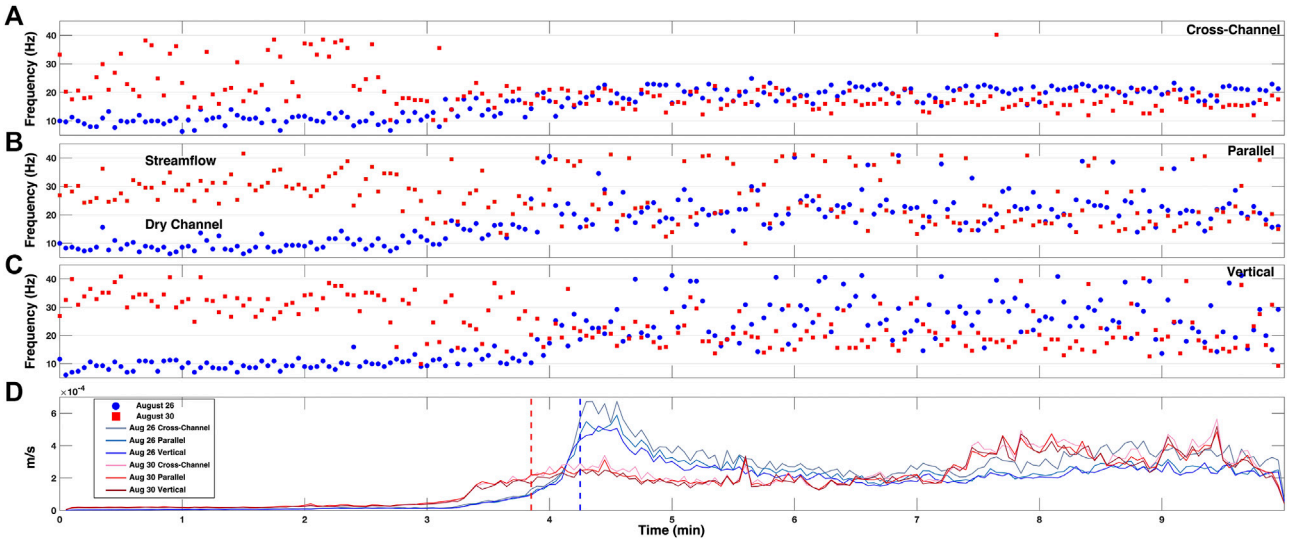

FIGURE 2 | (A–C) Peak spectral frequencies for both the August 26 (blue dots) and 30 (red squares) events containing pre-lahar (dry channel August 26, streamflow August 30) and first arrival. **(A)** cross-channel flow (E-component), **(B)** flow parallel (N-component), **(C)** vertical (Z-component), **(D)** RMS amplitude of the August 26 (blue lines) and 30 (red lines) events. Vertical ticks represent the time at which the first appearance of the lahar front is captured on the camera. All PSFs and RMS amplitudes were calculated using a 3 s time window.

direction. The installed video camera takes pictures every 3 s with 704 × 480 pixel resolution.

RESULTS

To examine the multi-component dynamics of the lahars, the recorded data were corrected for the instrument response before the maximum peak spectral frequency (PSF) amplitude, root mean squared (RMS) amplitude, and directionality ratios (DR) were estimated using a 3 s running time window. The 3 s time windows were acquired from a 10 min recording window around the head of the lahars as they passed the monitoring site (**Figures 2**, **3**) in each seismic component. Three second time windows were used to match the seismic data with the lapse time (3 s) between the camera imagery.

Multi-Component Peak Frequency Analysis

Examining PSFs in each flow direction, we use the frequency recorded at the maximum amplitude of the frequency spectra for each 3 s running time window. In this section, we describe only the August 26 and 30 events in detail, because of the differing nature of these events (dry channel/precursory flow) and their larger size compared to the other two events. For the August 26 lahar (**Figure 2**, blue plots) the dry channel/pre-lahar or background noise has a PSF around 10 Hz on average for all 3-components. When the lahar surge passes the monitoring station at ~4 min (**Figure 2D**, dashed lines) the PSF increases to above 15 Hz. Most notably, for the vertical (V) (**Figure 2C**) and the flow parallel directions (**Figure 2B**) there is a wide PSF range between 15 and 45 Hz. In the cross-channel direction (**Figure 2A**), the PSF distribution is more concentrated around 15–20 Hz.

The PSF for the August 30 lahar (**Figure 2**, red plots) contains two different flow types, with the precursory streamflow occurring before the lahar surge arrives. The streamflow cross-channel component (**Figure 2A**) has a range of PSFs between 15 and 40 Hz. The vertical (**Figure 2C**) and flow parallel (**Figure 2B**) directions have narrower PSF ranges between 25 and 40 Hz. When the lahar front is recorded seismically (~3 min, **Figure 2D**) the PSF of each component changes. The cross-channel PSF ranges between 15 and 20 Hz, which is similar to the August 26 lahar with the flow parallel and vertical components having PSFs between 10 and 40 Hz. In comparing the two types of flows on August 30, in the cross-channel direction the PSF changes from a wide (15–40 Hz) to a narrow range (15–20 Hz) when the lahar arrives. In contrast, the opposite is observed for the vertical and flow parallel directions, where the streamflow has a narrower (25–40 Hz) PSF range than the lahar (10–40 Hz).

In general, the differences between the lahars are small, the PSF ranges are similar for each component, where the cross-channel is 15–20 Hz (August 26, August 30), flow parallel is 15–45 Hz (August 26) and 15–40 Hz (August 30), as well as the vertical direction at 15–45 Hz (August 26) and 10–40 Hz (August 30). The most significant differences are seen at the range where the most dominant frequency bands or concentrations of PSF time windows exist for each component. The August 26 flow parallel direction (**Figure 2B**, blue dots) has a higher concentration of PSFs between 15 and 30 Hz with several time windows having PSFs up to 45 Hz. Moreover, the August 30 lahar (**Figure 2B**, red squares) has a PSF signature that is more bimodal than the August 26 event, where there is a lower range between 15 and 20 Hz and a higher range around 40 Hz. In the vertical component the August 26 event has a wide range of PSFs from 15

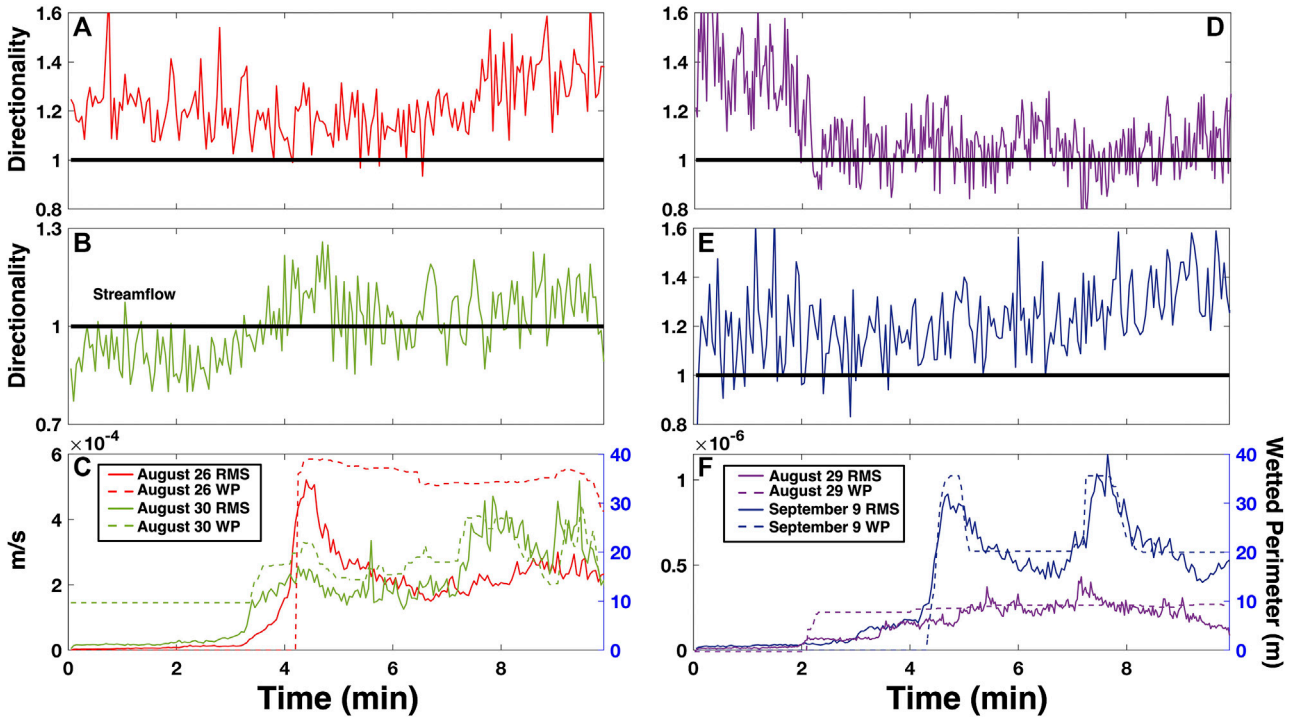

FIGURE 3 | Directionality ratio plots over time for the August 26 **(A)**, August 30 **(B)**, August 29 **(D)** and September 9 **(E)** events. Vertical RMS seismic signals and wetted perimeters for the August 26 and 30 events **(C)** and for the August 29 and September 9 events **(F)**. Wetted perimeters were estimated from video images and the known dimensions of Lumbre channel from digital elevation models (DEM). Video analyses used the imported measurements from the DEMs to estimate the height and width of each flow event for each 3 s lapse time of the camera.

to 45 Hz with no distinct pattern or concentration. The vertical component for the August 30 lahar on the other hand has a concentration of PSFs between ~15 and 25 Hz with several time windows encompassing PSFs up to 40 Hz. Finally, in the cross-channel direction, the PSF pattern for both lahars is similar with a narrow range between 15 and 20 Hz.

Directionality of Lahars

When analyzing mass flows using multiple component seismic data, one way to determine which flow direction has greater energy is through the directionality ratio (DR). The DR can be defined as the cross-channel divided by the flow parallel seismic amplitude. A $DR > 1$ indicates that the cross-channel energy is stronger than the flow parallel energy, and vice-versa for a $DR < 1$. The DR can be an indicator for many flow properties, including the wetted perimeter, amount of turbulent particle collisions, and sediment concentration (Doyle et al., 2010), which could yield evidence of flow rheology.

The DRs for a 3 s running time window for the 2016 events are shown in **Figure 3**. For the dense-front August 26 lahar (**Figure 3A**) the DR mostly stays above one for the entire 10 min recording duration. Furthermore, at ~7 min the DR increases to above 1.3. This increase late in the recording window is most likely becoming more positive due to an increase in concentration, amount of turbulent particle collisions and/or the channel beginning to incise (see **Supplemental Movie S1**), and not an increase in wetted perimeter, because the estimated wetted perimeter (**Figure 3C**, red dashed line) is less than when the lahar arrives. Furthermore, the dry channel bed/background noise also produces a $DR > 1$, indicating that the DR cannot be used for a potential real-time rheology change indicator for dry channels, at least for Lumbre.

For the August 30 event (**Figure 3B**), the precursory streamflow has a $DR < 1$, which then increases to a $DR > 1$ when the lahar surge passes the monitoring site. This switch from flow parallel to cross-channel dominance when the lahar arrives is possibly due to a larger wetted perimeter (**Figure 3C**, green dashed line) or an increase in sediment concentration (Doyle et al., 2010), and could be a potential real-time rheology change indicator for monitoring lahars. Additionally, even though the August 30 event has similar or increased seismic energy along with a lower wetted perimeter later in the recording window (after initial lahar front) than the August 26 event, the DR is ~0.2 less. This difference indicates that wetted perimeter cannot be the only factor in the determination of the DR.

During the August 29 event (**Figure 3D**) the DR remains around 1.0, which could indicate a smaller wetted perimeter or a lower concentration compared to the other events. From **Figure 3F** (purple lines), the amplitude and wetted perimeter are lower than the other events, but as also seen in the video analysis (**Supplementary Movie S2**) the lahar pulses show evidence of increased water content. When the second pulse occurs at ~7 min (**Figures 3D**,F, purple line) the $DR < 1$ indicates that the pulse may be a water wave with low particle

concentration. We also observe that the September 9 event (**Figure 3E**) is similar to the August 26 lahar in that the *DR* > 1 covers most of the duration and the wetted perimeters of the two pulses are comparable. Unlike the August 26 event, the September event is about two magnitudes smaller in seismic amplitude. Furthermore, the amplitude is smaller than the August 30 event, but has a larger DR. These differences could come from the fact that the September 9 event covered the entire width of the Lumbre channel which allowed for greater cross-channel compared to flow parallel seismic energy. Additionally, being able to flow over the entire channel width yielded a larger wetted perimeter than the August 30 event, which was mostly contained in the incised channel. Another possibility is that the sediment concentration could be higher for the September 9 event. The increased sediment conceivably came from erosion or entrainment of fine-grained material deposited by the August 30 event.

DISCUSSION

Comparing the PSF Response Between the August 26/30 Lahars

Examining the multi-component frequency content of the two main lahars in August 2016 shows that different flow types may play a significant role in the frequency spectra of the seismic signals. Additionally, each component details a different pattern in the frequency spectra, determined by many factors. As shown by others (e.g. Lai et al., 2018), the frequency range will increase as the lahar flows near and eventually passes the monitoring site. This can be seen for all three components (**Figures 2A–C**) in the dry channel scenario. As for the different flow types, each component has a differing frequency response and standard assessments from previous studies on just the vertical component cannot explain everything, but can help to understand what mechanisms may be causing these patterns.

As noted above, the August 26 lahar has a wider PSF range than the August 30 lahar in the vertical component (**Figure 2C**). This could be due to the August 26 lahar transporting larger clasts, which would make the bedload dominate the turbulent response, in turn creating higher frequencies (Schmandt et al., 2017). Furthermore, this same feature can be explained by the observations of Huang et al. (2004) who noted the PSF range increases with the mass of suspended clasts. Hence, the larger clasts of the August 26 event increases the PSF range because the grain size distribution becomes larger, thus creating a wider range within the flow from particle collisions to saltation effects. The vertical component of the streamflow has PSFs between 25 and 40 Hz where the flow is less turbulent and thus more capable of recording bedload transport produced frequencies (Doyle et al., 2010).

The difference in the flow parallel PSF pattern for the August 26 and 30 lahars (**Figure 2B**) may be explained by the flow parallel direction being more sensitive to flow processes, rather than bedload forces (Barriere et al., 2015), which would dampen the high frequencies of the August 26 event. Conversely, Coviello et al. (2018) showed that higher frequencies are more associated with fine-grained sediment transport. The August 30 event deposited fine-grained material all over the Lumbre channel (see **Supplementary Movie S3**) providing possible evidence for more time windows of higher PSF. Additionally, the August 30 lahar transported fewer large clasts compared to the August 26 event (see **Supplementary Movies S1, S3**), and PSFs created by particle collisions decreases with an increase in clast size (Huang et al., 2004; Burtin et al., 2009), which could be the cause of the August 30 event having a more bimodal PSF pattern than the August 26 event.

The PSF content in the cross-channel direction for the August 26 and 30 lahars (**Figure 2A**) could be due to the sizes of the lahars being similar or bedload processes having little to no influence on the frequency content. Conversely, the PSF signature for the streamflow may be due to the greater freedom of particle movement within the flow. When the sediment concentration decreases, the viscosity will decrease, creating a situation where fine grain particle collisions and interactions occur more, thus increasing the frequency content (Huang et al., 2004; Coviello et al., 2018). This opposing effect could also be due to the seismometer being installed according to the channel alignment, which could make the surface waves, in particular the Love wave nodes synchronize (lahar) or not (streamflow) with the location of the seismic station depending on flow type/energy. Furthermore, just the difference in the orthogonal forces on the channel walls could alter the frequency content.

The transition from streamflow to lahars (**Figures 2A–C**) shows a decrease in the PSF range, which could be caused by the transition from less solid to more solid content flowing by. If this were the case, the DR (**Figure 3B**) would increase from <1 to >1, because the cross-channel energy increases with an increase in sediment concentration (Doyle et al., 2010); which it does. This increase also suggests why the cross-channel frequency pattern is different from the other two directions. Doyle et al. (2010) showed that in the cross-channel direction, turbulence is more dominant than in the flow parallel direction, which could be why there is no scattering to higher frequencies seen in **Figure 2A** when the lahar arrives.

In the discussion above, we described many hypotheses of how differing flow processes or rheology may produce the recorded frequency response. Equally, other factors may also contribute to the seismic record of mass flows. Recently, others have shown (e.g. Coviello et al., 2019; Marchetti et al., 2019) that the energy of the source and the channel geometry play a significant role in the frequency response. High-friction channel beds, bends, and extreme elevation changes could all cause differing frequency responses produced by the same seismic source. Furthermore, background noise can cause "jumps" in PSFs, where each time window could be recording either the flow or background noise (Coviello et al., 2019). A potential cause for a bimodal response in the flow parallel direction can be produced by a moving source, where the seismometer records the flow before, as it passes, and after passing the sensor. Additionally, one of the more likely causes is the pulsatory nature of lahars, which could cause changes to the frequency spectra over the length of the event.

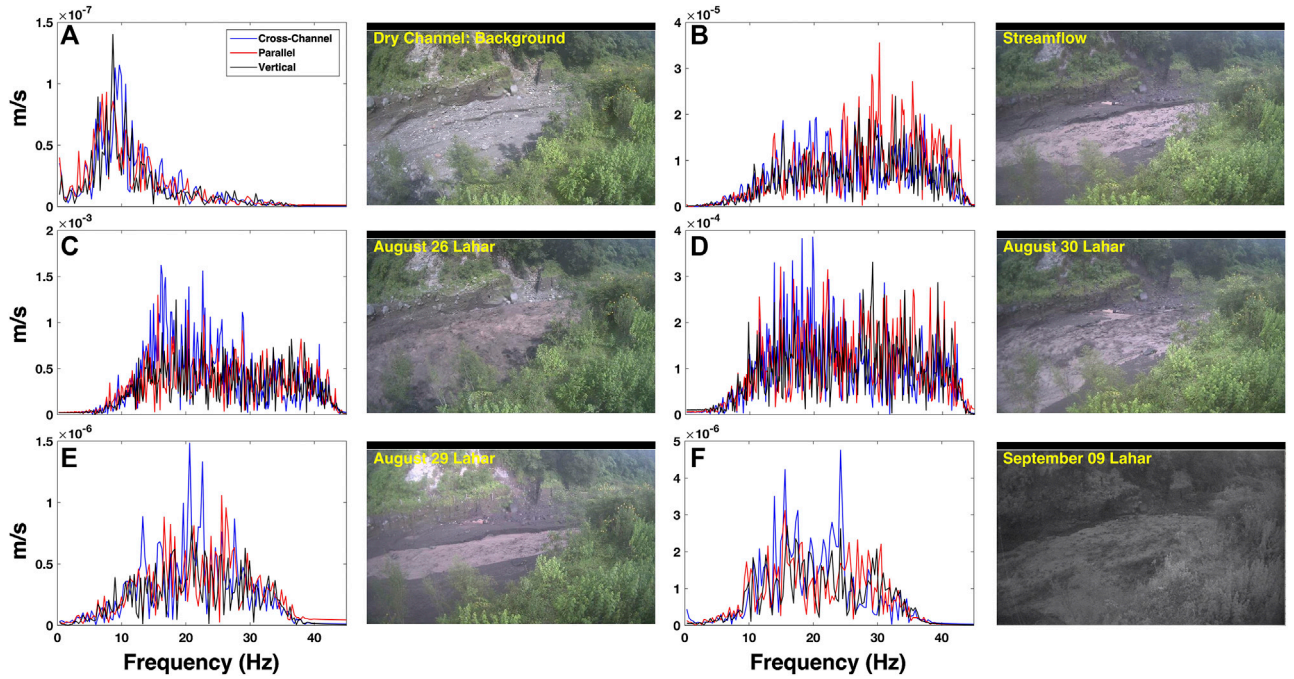

FIGURE 4 | Select 3 s multi-component frequency spectra with accompanying image of **(A)** dry channel, **(B)** streamflow, **(C)** August 26 lahar front, **(D)** August 30 lahar front, **(E)** August 29 lahar front, **(F)** September 9 lahar front for the cross-channel (blue), parallel (red) and vertical (black) directions. Note the amplitude difference between each frequency spectrum.

Spectral Analysis of Differing Regimes on Lumbre Channel

With a wide distribution of PSFs, we now investigate the entire frequency response of the flows by calculating full spectra for each 3 s time widow. For clarity, we only show a selected time widow for each event (**Figure 4**). From the full spectra, a pattern emerges from the different time windows during the 2016 events. The dry channel spectra (**Figure 4A**) depicts a low frequency (<10 Hz) response with little to no amplitude in the higher frequencies, typical of background noise (e.g. wind, environmental, etc.). The streamflow spectra (**Figure 4B**) has a shift to higher frequencies being more dominant. This is possible evidence that streamflow is more sensitive to bedload transport or less turbulent. Cole et al. (2009) showed that snow-slurry lahars on Ruapehu, New Zealand have higher flow parallel spectral amplitudes due to lower turbulence, and more lateral deposition, decreasing the cross-channel signal. Similarly, the streamflow on August 30 has increased amplitudes in the flow parallel direction, which suggests that the streamflow is less turbulent than the lahars. The August 26 frontal spectra (**Figure 4C**) is dominated by lower frequencies between 15 and 25 Hz with a drop in amplitude after this range. This effect may be caused by the lahar front being more sensitive to turbulence (Gimbert et al., 2014), sliding frictional effects of the front, creating lower frequencies (Huang et al., 2004), or higher sediment concentration (Doyle et al., 2010; Coviello et al., 2018). Conversely, the August 30 lahar front (**Figure 4D**) has a broad frequency spectra, which could be characterized as a combination of the low frequency August 26 event and the higher frequency August 30 streamflow. The broad frequency response of the August 30 lahar is similar to three lahars recorded on Mount Semeru, Eastern Java by Doyle et al. (2011), which was explained by the flows being less sensitive to flow properties (turbulence, viscosity), than to both frictional (lower frequency) and collisional (higher frequency) processes. If turbulence were dampened, the particles within the flow will have less influence on the basal shear stress, and the erosiveness of the flow would decrease (Doyle et al., 2011). This can be demonstrated by the August 30 lahar, which does not erode the channel but instead deposits fine grained material over the channel floor (**Supplemental Movie S3**). The August 29 event (**Figure 4E**) shows a dominant range of frequencies between 15 and 25 Hz, similar to the August 26 event. Differing, the August 29 event has a steep drop in amplitude at higher frequencies (>30 Hz), and the maximum peak frequency (~20 Hz) is higher than what was recorded for the August 26 event. The lack of higher frequency content is possibly from a smaller grain size distribution or a lower energy regime than the August 26 event, whereas the higher maximum frequency may be from a lower sediment concentration (e.g. Huang et al., 2004), as shown in **Figure 3D**, produced from a $DR \sim 1$. Furthermore, the September 9 event (**Figure 4F**) has a similar spectral pattern to the August 29 event, but with a bimodal peak frequency. The first peak frequency is at ~16 Hz and the second at ~22 Hz, which might signify two separate processes occurring. The lower peak could be related to flow processes such as freedom of particle movements (turbulence). The second peak at ~22 Hz may be a frictional process (bedload transport) similar to the August 26 event, in which a large block-rich front slides along a dry channel. Moreover,

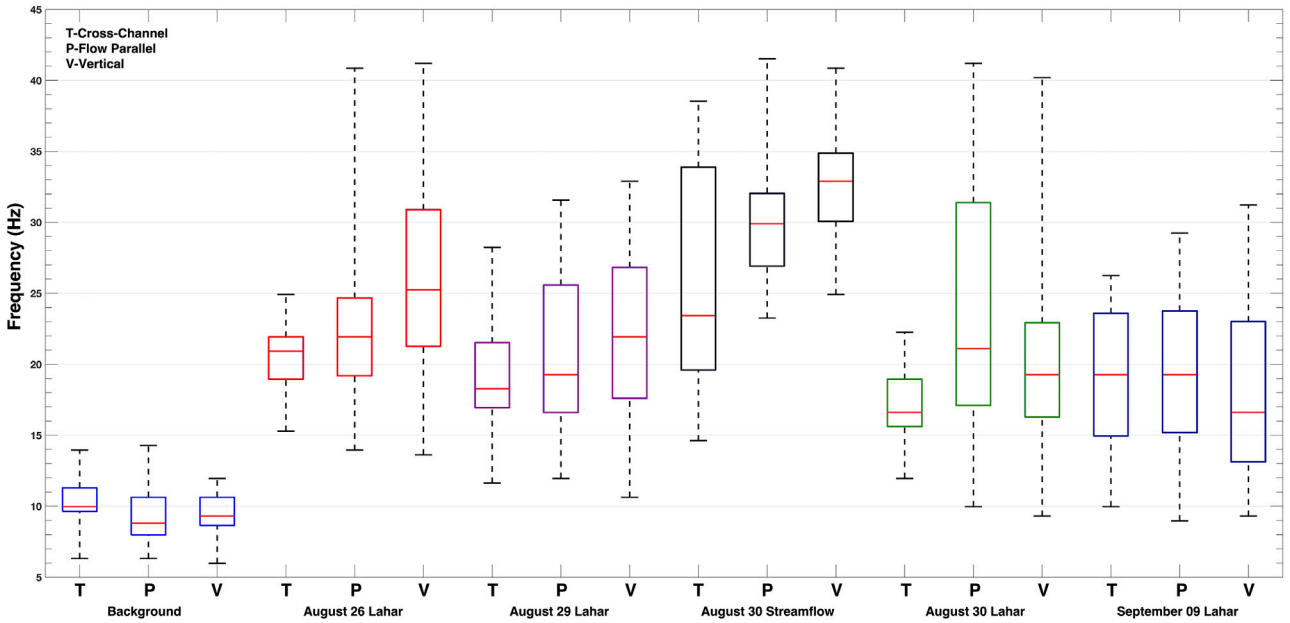

FIGURE 5 | Boxplots for peak spectral frequencies over the 10 min recording duration for each component for the background noise (blue), August 26 lahar (red), August 29 lahar (purple), August 30 streamflow (black), August 30 lahar (green), and September 9 lahar (navy).

the September 9 lahar has a high DR (**Figure 3E**) indicating a possible increase in concentration, which would decrease peak frequency as indicated by Huang et al. (2004). These two peaks are lower than the frequencies observed during passage of a hyperconcentrated flow in 2015, recorded with a geophone installed at the same location (Coviello et al., 2018). In that case, the high peak (70 Hz) was associated with sediment transport while the lower peak (30–40 Hz) was interpreted as flow turbulence. However, differing instruments, sampling frequencies, source energy, and channel conditions may have led to shifted spectral responses. The September 9 event flowed over the August 30 fine-grained deposits and was not channelized. The lahar was also smaller with less energy allowing the suspended grains more freedom to move and collide, producing higher frequency content, especially in the cross-channel direction.

The Implications of 3-Component PSF on Event Conditions

To obtain a more reliable comparison between each event, boxplots for each component and lahar event were created (**Figure 5**). The boxplots depict an evolution of the frequency content of the lahars over time at Lumbre. The cross-channel spectral content has a narrow interquartile range (IQR) for the August lahars, but becomes wider with the September lahar and the streamflow. This feature may be explained by channelization or freedom of movement, where the August 29 and 30 events were confined to the incised channel and the August 26 lahar was large enough to be confined to the Lumbre channel walls. Conversely, the lahar in September was not channelized and was free to flow side to side within the Lumbre channel. Compared to the streamflow, the September 9 event has a lower overall PSF IQR range, which could be explained by the freedom of fluid movement (channelization) as noted above, combined with higher turbulence and/or sediment concentrations compared to the streamflow shown by the increase in the DR (**Figure 3E**). Furthermore, since the streamflow was channelized, the wide IQR for the streamflow could instead be from the freedom of particle movement of smaller grain sizes within the flow, which would increase the overall PSF. The box plots for the flow parallel direction show that this component may be an indicator of erosiveness, i.e. where narrow IQRs may depict erosive regimes and wide IQRs indicate depositional regimes. The August 26 lahar has the smallest flow parallel IQR and eroded the channel bed creating the incised channel (**Supplemental Movie S1**), whereas the August 30 lahar deposited a layer of fine-grained sediment throughout the channel (**Supplemental Movie S3**). Furthermore, both the August 29 and September 9 events show a mix between depositional and erosional regimes, yielding similar IQR sizes between the extremes of the larger 2016 events. The vertical component boxplots for all the lahars have similar spreads, but **Figure 5** does show a decrease in median PSF over time. This pattern is possibly due to the change in channel bed composition by adding fine sediments (e.g. Huang et al., 2004). The August 26 and 29 events occurred on dry channels with little fine-grained material, whereas the August 30 event deposited fine-grained material, and the September 9 event flowed on top of these deposits decreasing the overall frequency.

Implications for Lahar Monitoring

The main goal of mass flow research is to progress the knowledge behind the properties and dynamics of flows for risk management and hazard warning. We show here that with

only one 3-component seismic station installed close to the channel (3 m) sufficient information was obtained for warning purposes. For example, the change in frequency distribution and DR when transitioning from streamflow to hyperconcentrated flow, the potential use of PSF to determine the depositional regime of a flow, and the increase in frequency when a lahar passes the monitoring station from a precursory dry channel. Using only one station does have its limitations, and installing more stations could benefit the results discovered here by showing whether or not these same features are universal in terms of both time and location. The seismic signals of mass flows are variable and strongly depend on where the station is, source-receiver distance, properties of the subsurface, properties of the channel, and flow properties and dynamics. For example, Schmandt et al. (2017) showed that there were differences in the seismic signals of stations installed on opposite sides of the channel from one another. This could affect not only the frequency response, but the amplitudes of the horizontal components, and thus the DR. Furthermore, flow dynamics and channel properties can and do change along the channel and having more stations along the channel could help to identify the characteristics of the flow. Doyle et al. (2011) used multiple stations along the same channel to show changes in lahars over time and station location at Semeru. Additionally, multiple stations along the channel allows the use of other techniques for detecting mass flows. Coviello et al. (2019) calculated the difference in seismic amplitudes of short and long period time windows to detect in real-time when a mass flow occurred.

The results from Volcán de Colima provide new data and show a practical application in using all three components, which can be used for monitoring, and that variabilities need to be accounted for before real world applications in systematic monitoring can be conducted. Using all three components for in depth frequency analysis and general hazard monitoring is beneficial in that there is important information in the horizontal components of the seismometer that should not be ignored. In earthquake hazards and geoengineering all seismic directions must be considered when building durable structures (e.g. buildings, bridges). Similarly, the construction of check dams and levees in flow channels should consider the horizontal energy from the mass flows. For risk management, using all available data needs to be considered by numerical modelers. Creating hazard models based on 3-component data could improve mass flow predictions due to the input of directional forces and patterns. Finally, in mass flow warning systems, we have shown that the DR and the distribution of PSFs can show regime changes within the channel, and that other information may be able to be obtained from the horizontal components (e.g. channelization, bedload transport). Overall, using all three components of the seismometer can enhance warning systems and yield results that single component instruments cannot.

CONCLUSION

Conducting a multi-component frequency analysis on lahars at Volcán de Colima, Mexico has yielded an understanding of which frequencies are dominant during differing flow types and processes. For the vertical and flow parallel directions, the transition from streamflow to a lahar coincides with a widening of the peak frequency distribution. This observation is reversed for the cross-channel frequency content, where the streamflow generates a wide frequency distribution, which then transitions to a narrow distribution as the lahars pass the seismometer. Furthermore, there is a drop in overall PSF when transitioning from streamflow to lahar. Component analyses demonstrated that channelization or freedom of movement in the cross-channel direction, bedload transport in the flow parallel direction, and channel bed composition in the vertical direction are possibly the main drivers in the PSF output of lahars. Conversely, with the number of variables that could affect the seismic signals produced by lahars, future assessments and data collection need to be conducted to solidify the observations discovered at Lumbre. Ultimately, the findings of this research may lead to better real-time monitoring of lahars, and lahar hazard assessment through the use of frequency analysis of all three components of the seismometer for dry channels, and especially channels with sustained flowing water.

DATA AVAILABILITY STATEMENT

The datasets generated for this study are available on request to the corresponding author.

AUTHOR CONTRIBUTIONS

BW performed seismic and video analyses and drafted the manuscript. LC and BW estimated wetted perimeter and frontal velocities of the flows. All participating authors contributed to the discussions and editing of the draft of the manuscript, as well as approving the final edition.

FUNDING

This work was supported by The Interdisciplinary Grant awarded by the Center of Natural Hazards and Disaster Science (CNDS), Sweden to BW, EARFLOW bilateral project granted to unibiz and CGEO-UNAM, funded by the MAECI (Ministero degli Affari Esteri e della Cooperazione Inernazionale) and the AMEXCID (Agencia Mexicana de Cooperación Internacional para el Desarrollo) to VC and the CONACyT-PN360 project to LC. We also recognize that this research would not be possible without support from the New Zealand Natural Hazards Research Platform and the Resilience to Natures Challenges (NSC), Volcano Program. We would also like to thank Kate Arentsen for editorial support.

SUPPLEMENTARY MATERIAL

The Supplementary Material for this article can be found online at: https://www.frontiersin.org/articles/10.3389/feart.2020.542116/full#supplementary-material

REFERENCES

Barriere, J., Oth, A., Hostache, R., and Krein, A. (2015). Bed load transport monitoring using seismic observations in a low-gradient rural gravel bed stream. *Geophys. Res. Lett.* 42, 2294–2301. doi:10.1002/2015GL063630

Burtin, A., Bollinger, L., Cattin, R., Vergne, J., and Nabelek, J. (2009). Spatiotemporal sequence of Himalayan debris flow from analysis of high-frequency seismic noise. *J. Geophys. Res.* 114, F04009. doi:F040090.1029/2008JF001198

Calvari, S., Tanner, L., and Groppelli, G. (1998). Debris-avalanche depostis of the Milo Lahar sequence and the opening of the Valle del Bove on Etna volcano (Italy). *J. Volcanol. Geoth. Res.* 87, 193–209. doi:10.1016/S0377-0273(98)00089-4

Capra, L., Borselli, L., Barley, N., Ruiz, J., Norini, G., Sarocchi, D., et al. (2010). Rainfall-triggered lahars at Volcan de Colima, Mexico: surface hydro-repellency as initiation process. *J. Volcanol. Geoth. Res.* 198, 105–117. doi:10.1016/j.jvolgeores.2009.10.014

Capra, L., Coviello, V., Borselli, L., Marquez-Ramirez, V., and Arambula-Mendoza, R. (2018). Hydrological control of large hurricane-induced lahars: evidence from rainfall-runoff modeling, seismic and video monitoring. *Nat. Hazards Earth Syst. Sci.* 18, 781–794. doi:10.5194/nhess-18-781-2018

Cole, S., Cronin, S., Sherburn, S., and Manville, V. (2009). Seismic signals of snow-slurry lahars in motion: 25 September 2007, Mt Ruapehu, New Zealand. *Geophys. Res. Lett.* 36, L09405. doi:10.1029/2009GL038030

Coviello, V., Capra, L., Vazquez, R., and Marquez-Ramirez, V. (2018). Seismic characterization of hyperconcentrated flows in a volcanic environment. *Earth Surf. Process. Landforms* 43, 2219–2231. doi:10.1002/esp.4387

Coviello, V., Arattano, M., Comiti, F., Macconi, P., and Marchi, L. (2019). Seismic characterization of debris flows: insights into energy radiation and implications for warning. *J. Geophys. Res.: Earth Surface* 124, 1440–1463. doi:10.1029/2018JF004683

Doyle, E., Cronin, S., Cole, S., and Thouret, J. (2010). The coalescence and organization of lahars at Semeru volcano, Indonesia. *Bull. Volcanol.* 72, 961–970. doi:10.1007/s00445-010-0381-8

Doyle, E., Cronin, S., Cole, S., and Thouret, J. (2011). Defining conditions for bulking and debulking in lahars. *GSA Bulletin* 123, 1234–1246. doi:10.1130/B30227.1

Gimbert, F., Tsai, V., and Lamb, M. (2014). A physical model for seismic noise generation by turbulent flow in rivers. *J. Geophys. Res.: Earth Surface* 119, 2209–2238. doi:10.1002/2014JF003201

Hürlimann, M., Coviello, V., Bel, C., Guo, X., Berti, M., Graf, C., et al. (2019). Debris-flow monitoring and warning: review and examples. *Earth Sci. Rev.* 102981. doi:10.1016/j.earscirev.2019.102981

Huang, C., Shieh, C., and Yin, H. (2004). Laboratory study of the underground sound generated by debris flows. *J. Geophys. Res.* 109, F01008. doi:10.1029/2003JF000048

Huang, C., Yin, H., Chen, C., Yeh, C., and Wang, C. (2007). Ground vibrations produced by rock motions and debris flows. *J. Geophys. Res.* 112, F02014.

Kean, J., Coe, J., Coviello, V., Smith, J., McCoy, S., and Arattano, M. (2015). Estimating rates of debris flow entrainment from ground vibrations. *Geophys. Res. Lett.* 42, 6365–6372. doi:10.1002/2015GL064811

Kogelnig, A., Surinach, E., Vilajosana, I., Hubl, J., Sovilla, B., Hiller, M., et al. (2011). On the complementariness of infrasound and seismic sensors for monitoring snow avalanches. *Nat. Hazards Earth Syst. Sci.* 11, 2355–2370. doi:10.5194/nhess-11-2355-2011

Lai, V. H., Tsai, V., Lamb, M., Ulizo, T., and Beer, A. (2018). The seismic signature of debris flows: flow mechanics and early warning at Montecito, California. *Geophys. Res. Lett.* 45 (11), 5528-5535. doi:10.1029/2018GL077683

Marchetti, E., Walter, F., Barfucci, G., Genco, R., Wenner, M., Ripepe, M., et al. (2019). Infrasound array analysis of debris flow activity and implications for early warning. *J. Geophys. Res.: Earth Surface* 124 (3), 567–587. doi:10.1029/2018JF004785

Pierson, T. (1985). *Initiation and flow behavior of the 1980 pine creek and muddy river lahars*. Mount St. Helens, Washington: Geological Society of America Bulletin, 1056–1069.

Roth, D., Brodsky, E., Finnegan, N., Rickenmann, R., Turowski, J., and Badoux, A. (2016). Bed load sediment transport inferred from seismic signals near a river. *J. Geophys. Res. Earth Surf.* 121, 725–747. doi:10.1002/2015JF003782

Schmandt, B., Gaeuman, D., Stewart, R., Hansen, S., Tsai, V., and Smith, J. (2017). Seismic array constraints on reach-scale bedload transport. *Geology* 45, 299–302. doi:10.1130/G38639.1

Surinach, E., Vilajosana, I., Khazaradze, G., Biescas, B., Furdada, G., and Vilaplana, J. (2005). Seismic detection and characterization of landslides and other mass movements. *Nat. Hazards Earth Syst. Sci.* 5, 791–798. doi:10.5194/nhess-5-791-2005

Thouret, J., Antoine, S., Magill, C., and Ollier, C. (2020). Lahars and debris flows: characteristics and impacts. *Earth Sci. Rev.* 201, 103003. doi:10.1016/j.earscirev.2019.103003

Tsai, V., Minchew, B., Lamb, M., and Ampuero, J. P. (2012). A physical model for seismic noise generation from sediment transport in rivers. *Geophys. Res. Lett.* 39, 2404. doi:10.1029/2011GL050255

Turowski, J., Wyss, C., and Beer, A. (2015). Grain size effects on energy delivery to the streambed and links to bedrock erosion. *Geophys. Res. Lett.* 42, 1775–1780. doi:10.1002/2015GL063159

Walsh, B., Jolly, A., and Procter, J. (2016). Seismic analysis of the 13 October 2012 Te Maari, New Zealand, lake breakout lahar: insights into flow dynamics and the implications on mass flow monitoring. *J. Volcanol. Geoth. Res.* 324, 144–155. doi:10.1016/j.jvolgeores.2016.06.004

Conflict of Interest: The authors declare that the research was conducted in the absence of any commercial or financial relationships that could be construed as a potential conflict of interest.